




# Low-temperature silver-based ink for highly conductive paths through industrial printing processes suitable for thermally sensitive substrates and beyond

Sandra Lepak-Kuc<sup>1,2,a)</sup> , Tatiana Nowicka<sup>1,3</sup>, Katarzyna Wasilewska<sup>1,3</sup>, Daniel Janczak<sup>1,2</sup>, Piotr Walter<sup>1,2</sup>, Małgorzata Jakubowska<sup>1,2</sup>

<sup>1</sup> Faculty of Mechanical and Industrial Engineering, Warsaw University of Technology, Narbutta 85, 02-524 Warsaw, Poland

<sup>2</sup> Centre for Advanced Materials and Technologies (CEZAMAT), Warsaw University of Technology, 02-822 Warsaw, Poland

<sup>3</sup> Masterpress S.A., Jacka Kuronia 4 Str., 15-569 Białystok, Poland

a) Address all correspondence to this author. e-mail: sandra.kuc@pw.edu.pl

Received: 31 July 2023; accepted: 6 November 2023; published online: 29 November 2023

Printed electronics is experiencing tremendous growth in applications and industry interest worldwide. One of the most frequently raised problems is the high curing temperature of commercially available conductive composites. This study describes the process of developing a customized low-temperature silver-based, conductive ink dedicated to the flexographic-printing technique. The formulation was optimized through a series of tests including printing trials, resistance measurements, evaluation of printed samples surface features, and mechanical properties. The appropriate ink viscosity, substrate compatibility, and sinterability at low temperatures were achieved. The dependence of the achieved conductivity on the type of raw materials used was also witnessed and described. The conductivity of the printed inks was evaluated for various polymer vehicles. Samples printed on flexible PET and paper substrates were thoroughly investigated; ink adhesion, scratch resistance, and performance after cyclic bending have been assessed.

## Introduction

The area of technology that combines electronics with printing techniques is known as printed electronics. The global printed electronics market is projected to grow from USD 9.9 billion in 2021 to USD 23.0 billion by 2026, at a cumulative annual growth rate (CAGR) of 18.3% from 2021 to 2026 [1]. The main goal of a final-printed electronics product development is to utilize the cheap and efficient reel-to-reel technology commonly used in the printing industry. The R2R process is a fabrication method of coating, printing, embedding, lamination, or other techniques onto a flexible substrate fed continuously from one roller onto another. Unlike sheetfed production, R2R printing is a continuous process that saves costs significantly, increasing flexibility, and production automation [2]. For that reasons, printed electronics focuses on the implementation of R2R technology for manufacturing of various electronic components being applied in the increasing applications, e.g., electrodes, antennas, wearable electronics, or sensors [3–12].

Flexography is one of the most universal printing techniques for flexible substrates. A characteristic feature of flexography is the usage of a flexible, convex printing form, usually made of a polymer, to transfer the liquid ink onto the substrate. These forms allow printing on a flexible substrate of any kind with the proviso that it shall not be perfectly smooth. Flexography can serve to print water-based (WB), solvent-based (SB) or UV-cured materials (UV). The necessity of fulfilling the range of specific requirements, apart from the materials' base, such as the size and number of conductive particles together with specific vehicle components affecting the inks' viscosity, printability, and transferability, as well as time, and temperature of the sintering process, provides a wide range of difficulty for conducting composite design [13–15]. It is important to note at this point that while flexographic technology is highly favored and promoted in the industry, in the scientific research on printed electronics, a different technology is prevalent which is screen printing [16–20]. This might result not only from the greater accessibility of screen printing, starting with low-cost manual equipment but

also from the ability to employ thicker composites with higher functional phase loading. Many scientific studies on selected flexographic parameters for printing conductive inks are also known [21–25]. Also, the use of flexographic printing has been described as a method to produce various structures for printed electronics applications [26–29]. However, this research is not comprehensive, and often commercially available inks are derived from pastes previously tested in screen printing. Nevertheless, existing functional materials and conductive pastes dedicated to screen printing are sometimes not optimal for efficient industrial printing processes. Some products are developed for flexographic printing, with the drying process parameters placed between 2 and 30 min in the temperature from 120 °C to 150 °C. The list of a selection of commercially available inks is shown in Table 1.

A market survey showed that several types of conductive inks are available: UV, SB, and WB. SB inks are more suitable for flexography than UV inks due to the possibility of creating thinner and more conductive layers.

Solvent-based conductive inks are based on a polymer–solvent vehicle with the addition of conductive particles as a functional phase. Conductive inks are mostly based on metal micro and nanoparticles. Silver flakes and nanoparticles (NPs) are most commonly applied in ink formulations due to their high electrical conductivity together with the fact that, unlike many other metals, their oxides are also conductive. The polymer matrix that binds the conductive particles is most commonly dissolved in an organic solvent with additives modifying the properties of the composition. The polymer/solvent ratio greatly affects the ink rheology; hence, it is dependent on the intended printing

method. The composition should guarantee the required electrical, mechanical, and rheological parameters. The binder ensures both the paste’s printability, i.e., the possibility of applying a layer in flexographic technology, as well as the proper adhesion of the applied layers to the substrate. The functional phase determines the electrical properties.

Functional materials need to be adapted to the process, and new process parameters need to be defined in terms of flexographic printing. This work focuses on the development of tailored ink formulation and its deposition by the flexographic technique. The optimal balance between conductive particle amount, ink viscosity, print conductivity, and drying conditions has been achieved. The research shows the suitability of prepared ink for industrial printing. A drying temperature below 100 °C and a printing speed of 100 m/min have been achieved, holding a great premise for industrial applications. To our knowledge, there are no papers describing the successful printing of silver conductive inks with a high-speed industrial press while using low-temperature drying that achieves high conductivity printing without additional processing [5, 30, 31]. Reports can be found describing the industrial-scale printing of graphene-based inks [32, 33], yet graphene-based inks provide much lower conductivity and are not suitable for printing electrodes or antennas. Research on silver-based conductive inks has been also reported, but described inks’ formulations are not tailored to the flexographic industrial printing or the printing process demands the special treatment of substrate and drying temperatures in a range of 150–300 °C [30, 34–38]. In our research, we are focusing on the development of materials for printing highly conductive layers as part of multilayer structures, such as NFC antennas

**TABLE 1:** Commercial conductive inks.

Nr	Trade name	Producer	Ink type	Printing technique	Drying T [°C]	Drying t [min]
1	124–02	Creative materials	WB	Flexographic	125	10
2	126–35	Creative materials	SB	Screen	120	5
3	108–6	Creative materials	UV	Screen	UV	
4	EXP 2652–40LT	Creative materials	SB	Inkjet	230	30
5	118–38	Creative materials	WB	Screen	175	10
6	Bectron 6680	Elantas	SB	Screen	120	10
7	Bectron 6671	Elantas	UV	Screen	UV	
8	DM-SIP-30615	Dycotec materials	SB	Screen	140	10
9	DM-SIP-3070S	Dycotec materials	SB	Screen	140	20
10	PFI-600	Novacentrix	WB	Flexographic	140	1
11	PFI-722	Novacentrix	WB	Flexographic	140	1
12	PSI-211	Novacentrix	WB	Screen	140	1,5
13	PSI-219	Novacentrix	WB	Screen	140	1,5
14	AFT 6700	Sun Chemical	WB	Flexographic	140	1
15	LOCTITE ECI 1011 E&C	Henkel	SB	Flexographic	150	10
16	LOCTITE EDAG PM 460A E&C	Henkel	SB	Screen	70	15
17	LOCTITE EDAG PD 004A E&C	Henkel	UV	Screen	UV	

and printed sensors. It is also worth pointing out that, although there are commercially available silver conductive inks for flexographic printing, they do require drying temperatures above 100 °C to achieve the desired electrical performance. Drying systems on standard industrial presses operate at temperatures around 100 °C. In order to dry at higher temperatures, therefore, costly modification of current production lines is required.

## Results and discussion

The first issue undertaken was to verify the influence of silver flake dimensions and their packing in the paste on electrical performance. For this purpose, a series of pastes using a single vehicle was prepared. A vehicle based on PMMA was selected, due to its published applicability within printing composites

[39, 40]. In consideration of the fact that the dimensions of the functional phase have a direct influence on its packing ability, pastes with different packing levels up to a relatively maximum were prepared for an in-depth analysis, whereby two values for the weight percentage packing levels were kept equal for both silver materials tested.

Two types of commercial silver flakes were used in this study: AX 20LC with an average diameter of approximately 2 μm by Amepox Microelectronics, Poland (hereinafter referred to as Ag 1) (Fig. 1 b) and the larger one with an average diameter of approximately 10 μm by Abraxas, Poland (hereinafter referred to as Ag 2) [Fig. 1(a)]. A composition containing Ag 1 was prepared with concentrations from 40 to 80 wt%. A composition containing Ag 2 was prepared with the silver flakes content from 20 wt% to 50 wt%. The sheet resistance of screen-printed

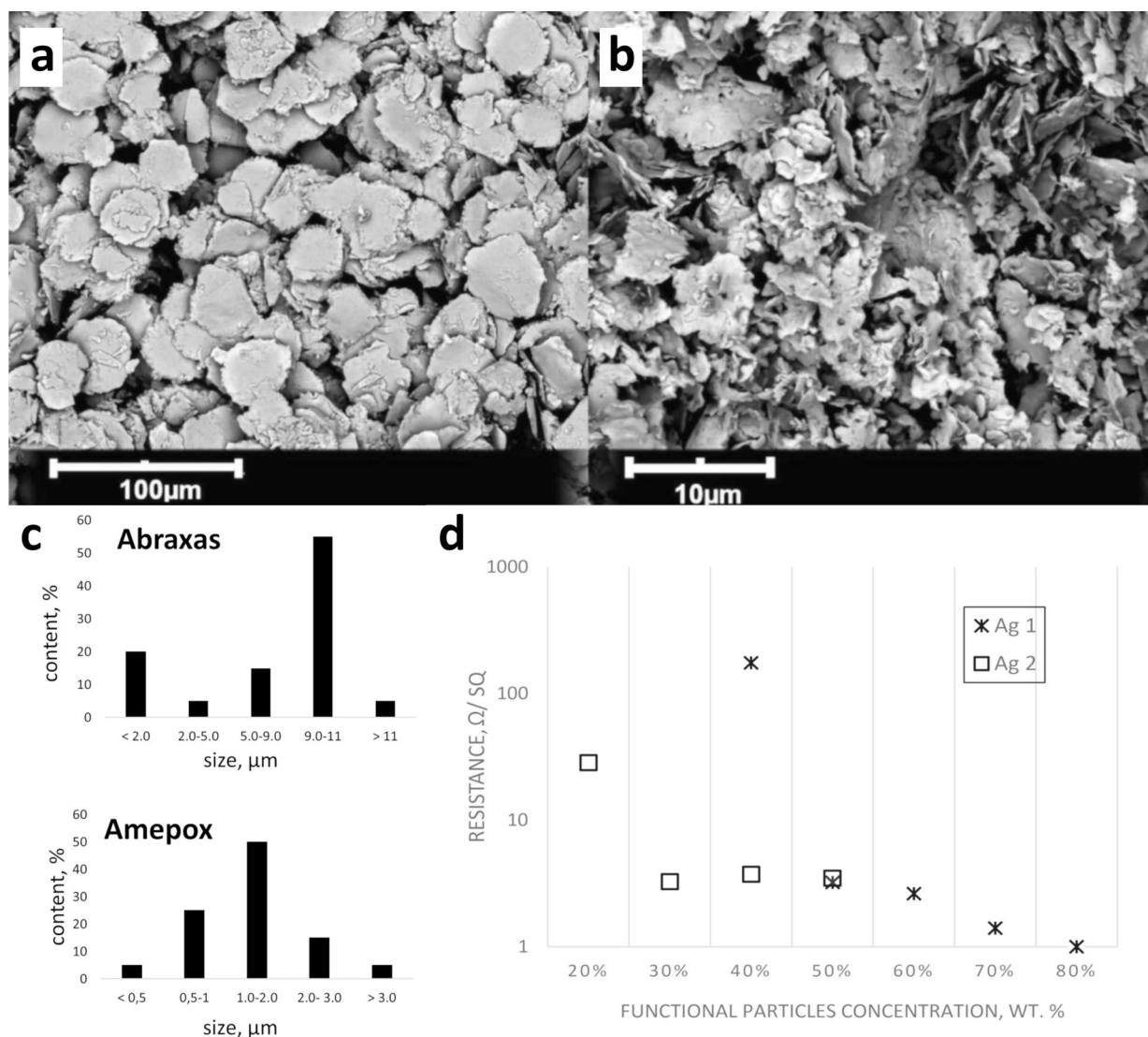


**Figure 1:** Features of used silver flakes: (a) SEM images of Ag 2 silver flakes (Abraxas,  $D \approx 10 \mu\text{m}$ ); (b) SEM images of Ag 1 silver flakes (Amepox,  $D \approx 2 \mu\text{m}$ ); (c) particle size distribution of Ag 2 (Abraxas) and Ag 1 (Amepox) silver flakes; (d) the influence of the functional particles' concentration in a composite on the surface resistance.

samples was evaluated after drying. The results are presented in [Fig. 1(c)].

For composition with a filling of 20 wt% of Ag 2 flakes, a conductive layer was obtained with a sheet resistance below 30  $\Omega$ /sq. For higher concentrations above 30 wt% of conductive particles, the resistance stabilized at the level of 3.5  $\Omega$ /sq. The concentration of 50% by weight was considered the maximum filling for this functional phase. For the Ag 1 flake-filled compositions, the layer resistance decreased in proportion to the increase in conductive particle content, down to less than 1  $\Omega$ /sq for a maximal filling set at 80 wt%. It has been reported that the use of larger silver phase flakes enables higher electrical conductivity to be achieved [41–43]. At the same time, however, as the particle size decreases, a higher packing of the functional phase is achievable. For instance, in our case, a difference between 50 and 80% by weight. This ultimately resulted in lower resistances for inks based on silver powder with smaller dimensions. In addition, it is notable that at a packing of 40%, considerably lower resistance values were obtained for the Ag 2-based tracks than for those based on Ag 1. This may indicate that a 40% packing with these small particles did not allow the conductive structures inside the path to be adequately connected everywhere. Flexography requires low-viscosity inks [44]. The rheological tests of ink formulations with different Ag 1 and Ag 2 contents were performed to confirm the suitability of the prepared samples for the flexographic-printing technique (Fig. 2).

According to the percolation theory, the conductivity of the composite increases with an increase in conductive particle concentration [45–47]. It should be noted that the surface resistance value for both compositions, containing 50 wt% of Ag 1 and 50 wt% of Ag 2 flakes, has the same value, but for small flakes, it is not a maximum concentration value. The maximum filling for Ag 1 silver flakes reaches 80 wt%. Therefore, in order to obtain better electrical parameters, a composition with a higher

functional phase filling should be generally used. However, in many cases where very high electrical conductivity is not a necessary condition, a composition with lower conductive particle concentration and a sparse connection network is used. In this way, economic benefits can be achieved when expensive fillers are used.

Based on those results, Ag 1 silver flakes with an average diameter of 2  $\mu$ m were selected for further tests as the functional material, allowing higher conductivity and better mechanical properties compared to larger flakes. Taking into consideration electrical properties, printability, and material cost, the optimal concentration in the composite was found to be 70 wt%.

As a next step, three ink formulations have been produced using binders B 1, B 2, B 3, and Ag 1 silver flakes. Printing attempts were undertaken on a laboratory scale using the flexographic-printing technique. The main objective of this step was to adapt the ink composition to the flexographic-printing process in terms of its printability. The printed samples were compared in terms of their electrical and mechanical properties. The appropriate surface, structure, and functional parameters should be achieved by the printed ink on the printing substrate. The surface should be smooth and uniform. The structure is understood as a shape and dimensions according to the printing form with sharp edges of the printed lines. The print should have also the correct dimensions specified in the print file [48, 49].

The best printability was found for the ink based on a B 3 [Fig. 3(a)]. The ink on B 1 had correct printability but weak adhesion to the PET substrate [Fig. 3(b)]. The B 2 vehicle showed a lack of suitability for the flexographic-printing technique due to the too-high ink surface tension, density, and viscosity. The appearance of the print and the flow of the ink prove the correct surface tension of both: the substrate and the ink. The surface tension of the substrate is maintained at the appropriate level by corona treatment. If the ink does not spread on such a prepared

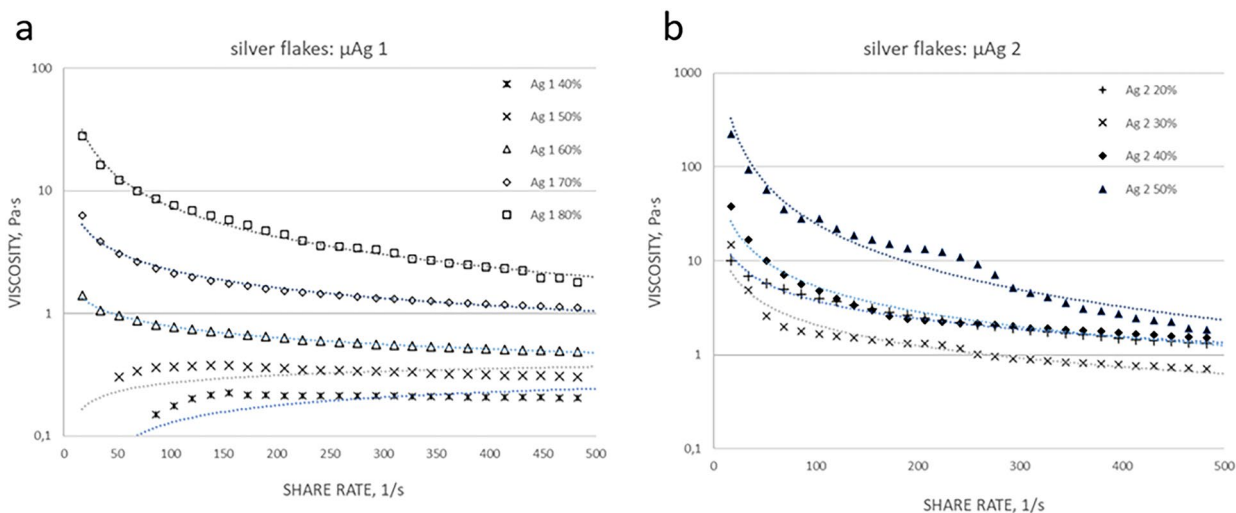


**Figure 2:** Viscosity diagrams of pastes containing: (a) Ag 1 silver flakes; (b) Ag 2 silver flakes.

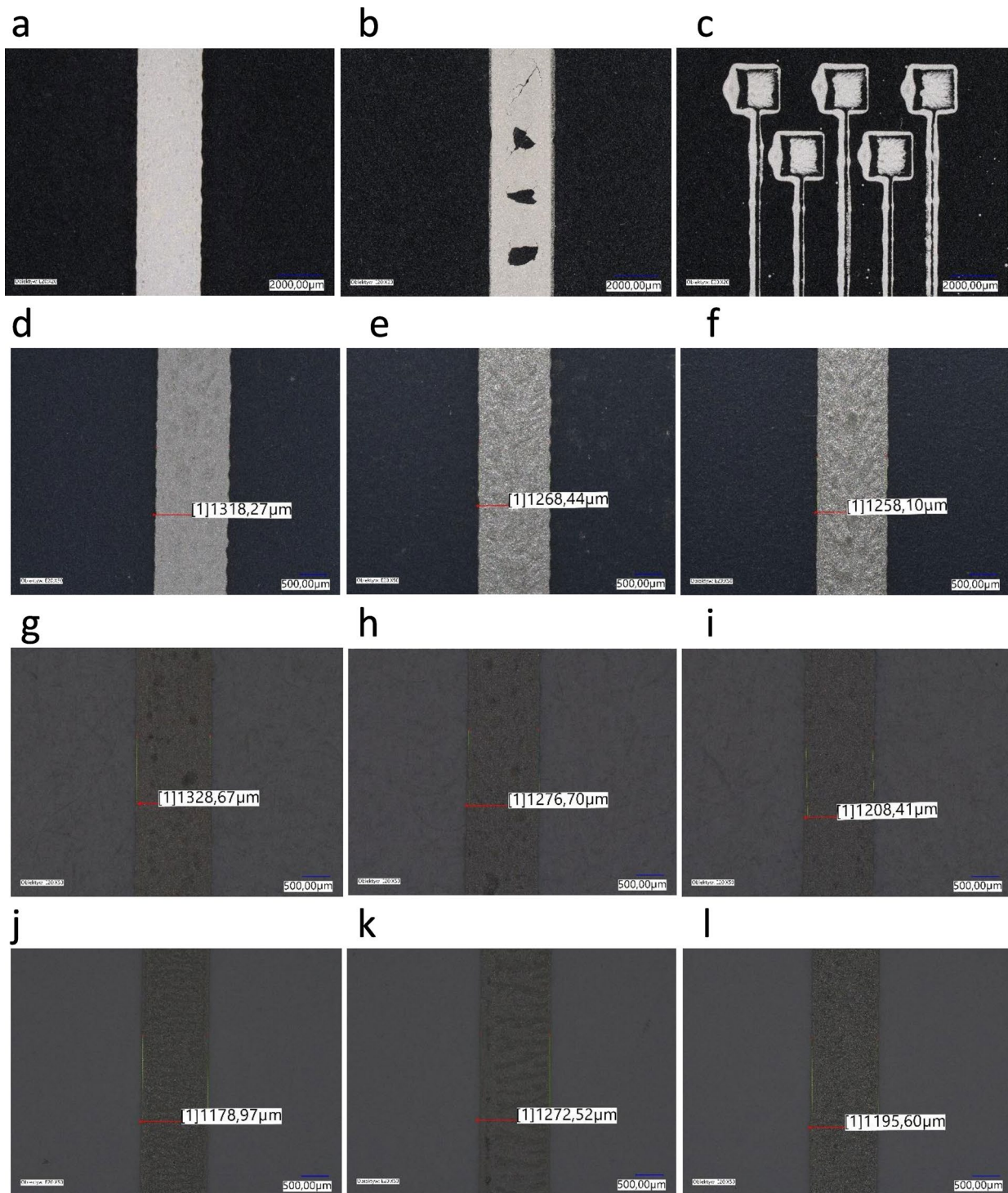


**Figure 3:** Digital microscope pictures of printed conductive tracks: (a) samples printed on PET substrate with the ink based on B 3 vehicle; (b) samples printed on PET substrate with the ink based on B 1 vehicle; (c) samples printed on PET substrate with the ink based on B 2 vehicle; (d) samples printed on PET with a printing speed of 25 m/min; (e) samples printed on PET with a printing speed of 50 m/min; (f) samples printed on PET with a printing speed of 100 m/min; (g) samples printed on paper with a printing speed of 25 m/min; (h) samples printed on paper with a printing speed of 50 m/min; (i) samples printed on paper with a printing speed of 100 m/min; (j) one layer printed on paper with the anilox roller 10 cm<sup>3</sup>/m<sup>2</sup>; (k) one layer printed on paper with the anilox roller 20 cm<sup>3</sup>/m<sup>2</sup>; (l) two layers printed on paper with the anilox roller 10 cm<sup>3</sup>/m<sup>2</sup>.

substrate, the surface tension of the ink is improper. The cohesive behavior of the ink proves its proper surface tension. A lack of flow and adhesion to the substrate were found. There was no continuity of the print, the ink was not transferred from the printing form to the substrate properly [Fig. 3(c)]. Measurement of the resistance for such a poor-quality print could have not been possible in a valuable form. Based on those results, binder B3 was chosen for the final ink formulation. The boiling points of used solvents provide the best drying features for the used drying method. The B3 formulation provides the best elasticity, surface tension, and viscosity of the final conductive paste during the flexographic printing, which was observed during the application process. For further trials, an ink sample was prepared with a 70 wt% ratio of Ag 1 silver flakes and 30 wt% of B 3 binder (hereinafter referred to as TK0018). In rheological tests, this paste showed the desired shape of the shear-thinning curve and for shear rates of 15 1/s, 100 1/s, and 400 1/s exhibited respectively viscosities of 41.1 Pa·s, 21.8 Pa·s, and 3.6 Pa·s.

The final ink composition was tested under both laboratory and industrial conditions. The tests were carried out in a standard production environment, which means an ambient temperature of 23–25 °C, and relative air humidity of 40–50%, on a standard roll flexographic machine with a printing speed of 25 m/min, 50 m/min, and 100 m/min. Samples printed on different substrates with different ink transfers were evaluated using a digital microscope. A smoother surface was noted on the paper substrate, yet there was greater size variation. Concurrently, better size stability was obtained on the PET film both in the laboratory and in the industrial press. Increasing the speed of the R2R process provided better dimensional stability, which is consistent with existing reports [33]. The lowest dimensional deviations were obtained at the highest printing speed of 100 m/min [Fig. 3(d–i)]. One of the challenges to overcome when developing industrial technology is finding a balance between efficient process speed and adequate print quality.

The ink transfer from the ink tray to the substrate is carried out via a raster roller. The number, size, and geometry of the cells engraved on the roller determine the volume of the raster roller and the amount of ink that will be transferred to the substrate. The greater the volume of the raster roller ( $\text{cm}^3/\text{m}^2$ ), the greater the transfer. The raster rollers described in the methodology section were used to carry out the tests, and the transfer of conductive ink from 2.2  $\text{g}/\text{m}^2$  to more than 13.3  $\text{g}/\text{m}^2$  was assessed. At higher ink transfers, overloaded print can occur due to too large a volume of raster roller cells. It is very important to determine the maximum ink transfer to maintain adequate print resolution. With poor ink transfer, small unprinted areas were noted. Images of compared samples with different ink transfers are shown in [Fig. 3(j–l)].

The print topology on PET and paper substrates was assessed through contact profilometry for each type of anilox

roller. The results indicate a strong correlation between layer thickness and the roller volume for 20–40  $\text{cm}^3/\text{m}^2$  values. For anilox rollers 6.5–12  $\text{cm}^3/\text{m}^2$ , however, no significant influence of roller engraving was found on both layer thickness and surface roughness values. This fact is related to the ink transfer from the anilox roller cells to the printing substrate. In the case of anilox rollers of volume 6.5–12  $\text{cm}^3/\text{m}^2$ , the level of ink transfer is comparable and is within the range of 2.2–4  $\text{g}/\text{m}^2$ . In the case of volumes 20  $\text{cm}^3/\text{m}^2$  and 40  $\text{cm}^3/\text{m}^2$ , the ink transfer is much higher—6.7  $\text{g}/\text{m}^2$  and 13.3  $\text{g}/\text{m}^2$ , respectively. This directly affects the thickness of the printed layer. A rougher print surface was noted on the paper due to the greater roughness of the substrate itself.

All prints on PET substrate showed excellent ink adhesion, scratch, and bending resistance at level 1 of the used evaluation scales. The prints on a paper substrate had a weaker scratch resistance at level 2, but the same bending resistance at level 1. The ink adhesion test with the adhesive tape could be performed only on a plastic substrate since adhesive tape destroyed the paper. The experimental data are presented in Fig. 4.

Figure 4 shows what mechanical strength values characterize the prints in measurements of adhesion to the substrate, scratch test, and bending resistance. A detailed description of the evaluation scales can be found in the Methods section. For the paper substrate, the adhesion measurement by the applied test cannot be acknowledged due to the detachment of the substrate itself with scotch tape.

The electrical parameters of the printed samples were measured and compared according to the materials used and to the process parameters, such as printing speed, drying conditions, and ink transfer. Electrical performance depends on, among others, a printed layer thickness. The required thickness of the printed layer is achieved by using proper ink transfer. As it was mentioned above, ink transfer in flexographic printing is provided by an anilox roller. The measured resistances depending on the roller used are shown in [Fig. 5 (a)]. The results depending on the different speeds for the R2R printing are presented in [Fig. 5(b)].

It was noted that a higher conductivity was obtained on the PET substrate. This is due to the low absorption of the film substrate. The paper substrate can partially absorb the conductive ink before drying, resulting in a lower conductivity of the print. For low transfers, it may even result in a complete lack of conductivity on the paper. As shown in [Fig. 6(a)], for a roller raster of 6.5  $\text{cm}^3/\text{m}^2$ , samples printed on paper are not electrically conductive. With R2R printing, higher conductivities were also obtained on the PET substrate. In R2R trials, the printing speed's influence on the printed tracks' conductivity was observed. The higher the speed, the lower the conductivity. Increasing the printing speed results in a shorter time for the conductive ink in the tunnel. In this case, less solvent evaporates and the high

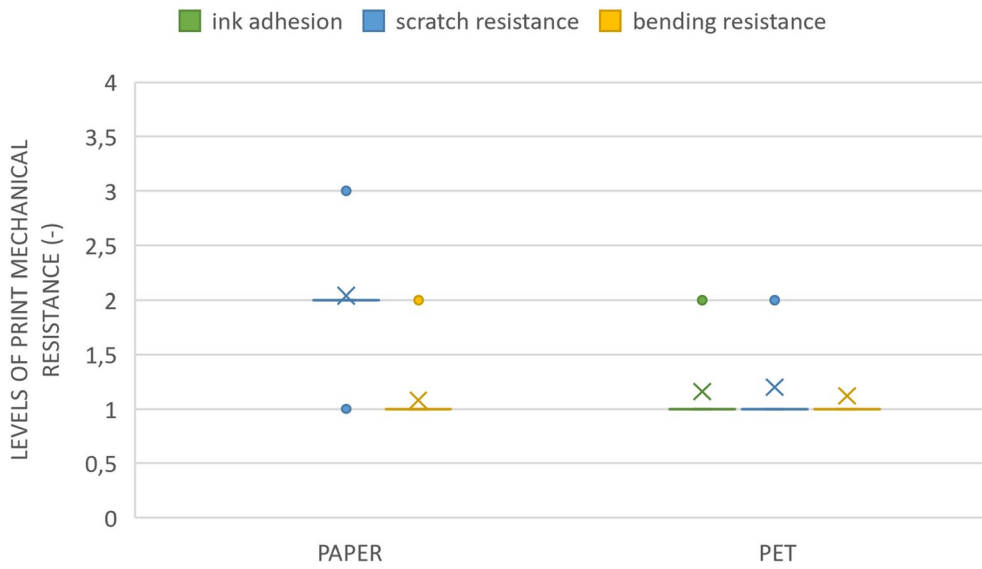


**Figure 4:** Mechanical resistance of prints on paper and PET substrates after ink adhesion, scratch, and bending resistance tests. The X symbol represents average values, short horizontal bars illustrate the values of samples majority, dots show the minimum and maximum values.

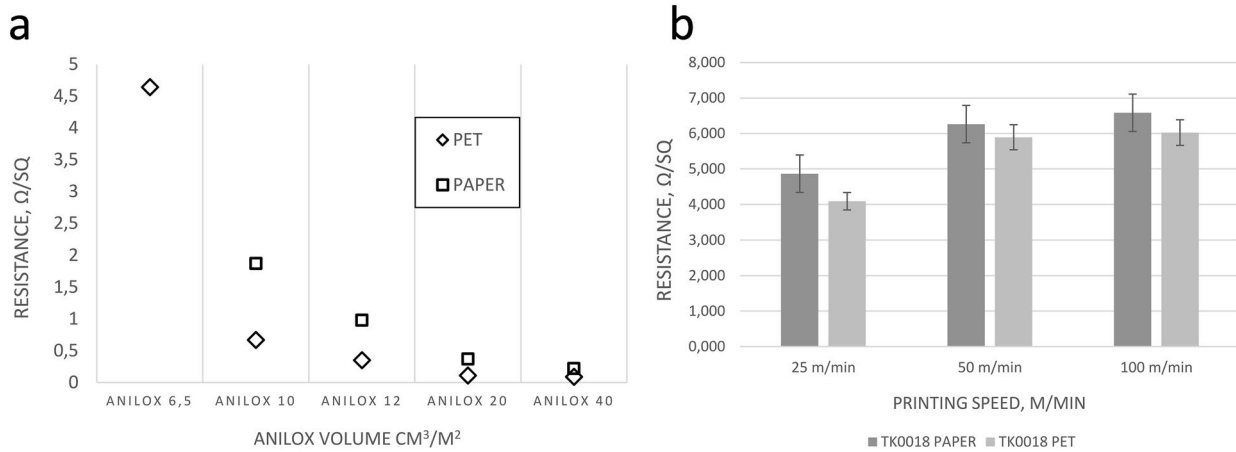


**Figure 5:** Resistance of conductive paths: (a) printed with different aniloxes; (b) printed with different speeds.

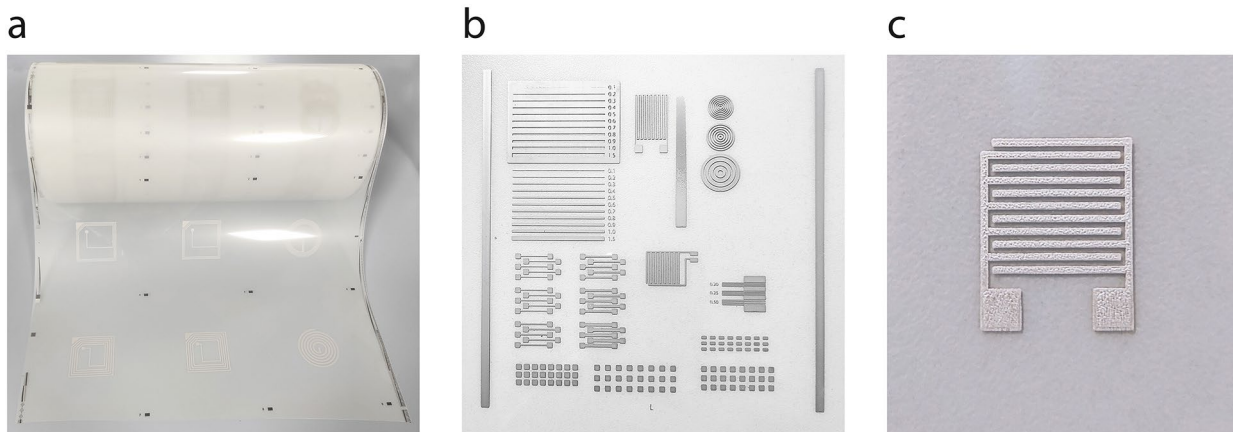


**Figure 6:** Examples of patterns of conductive elements flexographically printed on flexible substrates for various applications: (a) NFC antennas, (b) conductive tracks, and contact pads for hybrid electronics, (c) electrodes.

temperature interacts with the conductive particles for a shorter time. The binder material could still stay between conductive particles, and thus, fewer conductive connections are formed, which ultimately leads to a decrease in conductivity.

Different drying temperatures have also been checked. The drying process on a flexographic press takes place in a tunnel with hot air. The temperature could be adjusted in a range from 50 °C to 100 °C. The trial started with the lowest temperature usually used in a standard packaging industry printing process—50 °C. No conductivity was registered on a print. This range of drying temperatures is too low to ensure efficient solvent evaporation and conductive particles sintering. The initial conductivity was achieved at a temperature of 70 °C. The average registered resistance was 9.83 Ω/sq. The conductivity was improved with temperature increasing up to 90 °C. Then the average registered resistance was 4.37 Ω /sq. In industrial printing, the better dimensional stability of the printed structures was found. Increasing the printing speed reduces the time between ink application and drying unit. That limits the ink spreading on the substrate surface and results in better-preserved printed paths width. With lower printing speed, the ink enters the drying tunnel later and has more time to penetrate the substrate, which results in wider printing paths. The acceptable width deviation was about 10% in comparison to the printing file. At the lab scale, the average width deviation was 30%.

Examples of the printed samples are shown in Fig. 6.

## Conclusion

The developed ink formulation is adaptable by modifying silver flake ratios, silver flake sizes, polymer binder, and solvent components. Each such modification may result in a shift of electrical parameters, but also in a different print quality. From among all the investigated in this study, the best results in terms of ink printability and print parameters were obtained with 70 wt% packing of silver flakes with an average diameter of 2–4 μm in a binder consisting of 34 wt% Laroflex MP35 polymer in a mixture of solvents: 2-(2-butoxyethoxy)ethyl acetate and 2-butoxyethanol (70:30). In the context of the test substrates, better electrical performance, dimensional stability, and mechanical properties were reported on the plastic (PET) substrate. For paper, larger dimensional deviations and lower conductivity were observed. Such a result is most likely caused by the absorption of the ink into the substrate. Coated paper and plastic substrates are recommended if higher conductivity is required.

The efficiency of the developed ink was confirmed in print quality tests on an industrial flexo press. Tests showed that an ink transfer of more than 4 g/m<sup>2</sup> is required for solvent-based inks. The best result in terms of electrical conductivity was achieved at a speed of 25 m/min with a tunnel drying

temperature of 90 °C. However, the process also can be carried out at speeds up to 100 m/min with the same temperature of 90 °C. Inferior electrical performance is recorded in that case, but better printing geometry is obtained. The average printing resolution for the R2R process is in the range of 0.1–0.2 mm. The recorded layer sheet resistance for samples printed at 25 m/min was found to be ≈ 4.0 Ω/sq on a PET substrate and ≈ 4.8 Ω/sq on coated paper. During the trials, there was no possibility of achieving higher temperatures on a typical industrial flexographic press at the factory, where tests were conducted. Possibly better conductivity could be achieved with drying at 120 °C or 150 °C. However, the production line needs to be customized and the power consumption on a production line will increase significantly then. It will negatively affect the cost of production. The balance between the quality of the print (resolution, conductivity) and the costs (printing speed, temperature in the tunnel) needs to be kept. The research showed that drying with a temperature of 90 °C allows the achievement of appropriate conductivity for the range of applications. The study demonstrated the feasibility of using flexographic-printing techniques and custom ink compositions for high-performance processing of low-cost, flexible-printed conductive paths, electrodes, and sensors. The developed ink enables the printing of a range of electrically conductive patterns, allowing the production of printed antennas, and detectors, like humidity or temperature, or ECG electrodes. The developed ink formula and the method of its manufacture have received patent protection.

## Preparation, materials, and experimental methods

Three polymers were tested: thermoplastic polyurethane elastomer 37 Shore A based on polyesters (hereinafter referred to as TPU), poly(methyl methacrylate) polymer  $M_w \approx 350.000$  (hereinafter referred to as PMMA), as well as Laroflex MP35 resin (hereinafter referred to as LA). Selected polymers were dissolved in the following solvents: dimethylformamide pure for analysis (p.a.) (DMF) and tetrahydrofuran p.a. (THF) were used to dissolve TPU, PMMA was dissolved in [2-(2-Butoxyethoxy)ethyl] acetate p.a. and LA in a mixture of [2-(2-Butoxyethoxy)ethyl] acetate p.a. and 2-Butoxyethanol p.a. In addition, other solvents have been used to modify the properties of the polymer paste, such as acetone, toluene, or dichloromethane (DCM). TPU and LA were purchased from BASF Lampertheim GmbH, Germany, and the rest of the mentioned compounds were purchased from Sigma-Aldrich Chemie GmbH, Germany.

Two types of commercial silver flakes were used in this study: Ag 1–AX 20LC with an average diameter of approximately 2 μm by Amepox Microelectronics, Poland and Ag 2 with an average diameter of approximately 10 μm by Abraxas, Poland.



Coated paper Sappi Galerie Art Silk 170 g/m<sup>2</sup> by Sappi and PET film MYLAR A 174 g/m<sup>2</sup> by DuPont have been chosen as substrates for printing tests.

### Ink formulation

The laboratory procedure for producing conductive silver paste consists of two stages.

The first step is vehicle preparation. In all cases, the polymer dissolution process was carried out at the temperature of 40 °C using a magnetic stirrer at the speed of 200 r/min (revolutions per minute). The processing time did not exceed 48 h. The appropriate solvent mixture is a key factor for the hardening of the printed layer and defines the drying conditions. The main parameter that needed to be taken into consideration is the boiling point of the solvent. In the end, the optimal ratio of high-boiling solvents and low-boiling solvents was found. The boiling points of the used solvents are presented below in Table 2.

The composite tests were conducted in two sections. In the first, vehicles on high-boiling solvents were prepared and tested for printing and electrical parameters in screen-printing technology. Composite binder consisted of a polymer and compatible solvent. Three polymer–solvent variants were chosen as composite binders and were mixed in the ratio as below:

- 8 weight percent (wt%) PMMA Mw ≈ 350.000 in [2-(2-Butoxyethoxy)ethyl] acetate (hereinafter referred to as B 1)
- 15 wt% TPU in a mixture of DMF: THF (50:50) (hereinafter referred to as B 2)
- 34 wt% LA in a mixture of [2-(2-Butoxyethoxy)ethyl] acetate: 2-Butoxyethanol (70:30) (hereinafter referred to as B 3).

In the next section, the composites to be tested on flexographic printing were obtained by adding lower boiling solvents.

In the second step of the paste preparation procedure, the conductive material was added to the prepared vehicle. To break up agglomerates, silver flakes were subjected to the initial sonication procedure in acetone in a 300 W ultrasonic cleaner for 1 h, and then, after the initial evaporation of the solvent, they were heated at 250 °C for another hour to remove any lubricants

**TABLE 2:** List of used solvents with their boiling points.

Solvent	Boiling point [°C]
Dimethylformamide (DMF)	153
Tetrahydrofuran (THF)	66
2-(2-Butoxyethoxy)ethyl] acetate	246
2-Butoxyethanol	171
Acetone	56.05
Toluene	110.6
Dichloromethane (DCM)	39.6

thermally. Homogenization of the composite paste in the first section was performed manually in an agate mortar for 15 min with constant control of the weight of the composite to eliminate any solvent deficiencies. In the case of pastes dedicated to flexographic printing, with reduced drying temperature, based on a mixture of higher and lower boiling solvents, it was necessary to develop a special procedure to minimize the undesirable process of evaporation of low-boiling solvents during the dissolution of polymers. The procedure was based on the preparation of a precursor with a higher polymer content first, and then, after cooling the precursor, adding a defined amount of a solvent with a lower boiling point. In addition, pastes with reduced drying temperature with low-boiling solvents were grounded in a mortar in a cool environment. In the case of DCM with a very low boiling point, solvent deficiencies were replenished in the middle of the paste-grinding process. The solvent evaporated during the process due to the energy required in the grinding. After the production process, the pastes were placed in polypropylene containers with an additional parafilm seal.

### Printing methodology

Two printing techniques were involved. Screen printing during the ink formulation process was performed on a precise automatic printer Aurell C920 with a 77 T polyester screen. The final evaluation of developed recipes has been made using the flexographic-printing technique on a Testacolor 171 device produced by NSM. Samples were printed on sheets of substrates 170 × 200 mm. The constant printing speed of 10 m/min was maintained. The flexographic-printing unit was equipped with steel anilox rollers. The surface of each anilox roller was covered by ceramics based on chromium oxide. All used anilox rollers had the 60 degrees hexagonal pattern. This pattern is the most common engraving due to its performance advantages. The 60 degrees hexagonal pattern allows for a maximum number of cells to be placed on the anilox roller's surface and provides the most efficient ink transfer. Each anilox roller in the set had different volumes (cm<sup>3</sup>/m<sup>2</sup>) and line counts (l/cm) provided different ink transfers: (1) volume 6.5 cm<sup>3</sup>/m<sup>2</sup> with line count 260 l/cm and estimated ink transfer of 2.2 g/m<sup>2</sup>; (2) volume 10 cm<sup>3</sup>/m<sup>2</sup> with line count 160 l/cm and estimated ink transfer of 3.3 g/m<sup>2</sup>; (3) volume 12 cm<sup>3</sup>/m<sup>2</sup> with line count 140 l/cm and estimated ink transfer of 4 g/m<sup>2</sup>; (4) volume 20 cm<sup>3</sup>/m<sup>2</sup> with line count 50 l/cm and estimated ink transfer of 6.7 g/m<sup>2</sup>; (5) volume 40 cm<sup>3</sup>/m<sup>2</sup> with line count 28 l/cm and estimated ink transfer of 13.3 g/m<sup>2</sup>.

The ASHAI BFTH polymer plates were used. Plates were mounted to the printing cylinder with TESA TAPE-73422-620. The Longlife doctor blades were used in an open doctor blade system.

The Binder FD 115 chamber has been used to dry the solvent-based materials offline.

Next, an industrial printing machine Varyflex by OMET in the R2R process was used to print the most promising material. The standard tooling of the flexographic-printing unit was used: anilox rollers, polymer plates, and doctor blades mentioned above. The drying process took place online on a printing press. The process was carried out with different printing speeds of 25 m/min, 50 m/min, and 100 m/min.

### Measurement methods

The printed layers were designed to evaluate different properties of the printed samples as printability, print geometry, surface topography, adhesion to the substrate, bending, and scratch resistance as well as conductive properties.

### Printability, print geometry, and surface topography

Digital microscope VHX-7000 Keyence was used to observe printed artwork. The surface was observed with the lenses E20 and E100 with  $\times 50$ ,  $\times 80$ ,  $\times 200$ , and  $\times 300$  zooms. Printed elements have been measured using lenses E20  $\times 50$ , and E20  $\times 80$ , and their size was compared to the size established in the printing file. The average value from 5 samples was used for dimensions' evaluation of measured printed elements.

The prints' layer thickness and surface topography were assessed through contact profilometry using Bruker DektakXT stylus profiler with a motorized XYR stage and microporous, ceramic vacuum worktable. The stylus with a tip radius of

12.5  $\mu\text{m}$  was used for all the measurements. To ensure not to scratch the surface in the scanning process, the stylus force was set to 5 mg, equivalent to  $4.9 \times 10^{-5}$  N. Horizontal resolution along the scan direction was 0.11  $\mu\text{m}/\text{pt}$ , while the device's vertical scan range was set at 65.5 mm which corresponds to stylus inducer performing at a 1 nm resolution.

Scan locations and profile analysis were carried out with a semi-automated procedure to ensure the comparability of the results. For each substrate, the indicated corner of the first 0.5-mm-width trace was located and used as an origin point (A) for the positioning. The second corner point (B) was located to align the printed trace perpendicularly to the stylus scan by automated alignment by the rotary axis. Three scans were performed automatically, spaced 1.5  $\mu\text{m}$  apart symmetrically to the center of the printed path [Fig. 7(a)]. Considering the width trace of 500  $\mu\text{m}$ , the scans of a 1000  $\mu\text{m}$  length started 250  $\mu\text{m}$  below the A, B axis so that the printed surface was the central segment of the scan [Fig. 7(b)].

After the scan, the roughness and height of the layer were calculated as follows. Segments of 200  $\mu\text{m}$  at each end of the scan, corresponding to an unprinted substrate surface, were used to level the profile characteristic and set a zero point for height estimation. Central 500  $\mu\text{m}$  of the profile, consisting of the printed layer, was used to calculate the average height (layer thickness) and arithmetic average roughness ( $R_a$ ).

### Ink adhesion to the substrate

Ink adhesion assessment was done according to the FINAT method no. 21—tape test. Twenty-five samples printed on PET

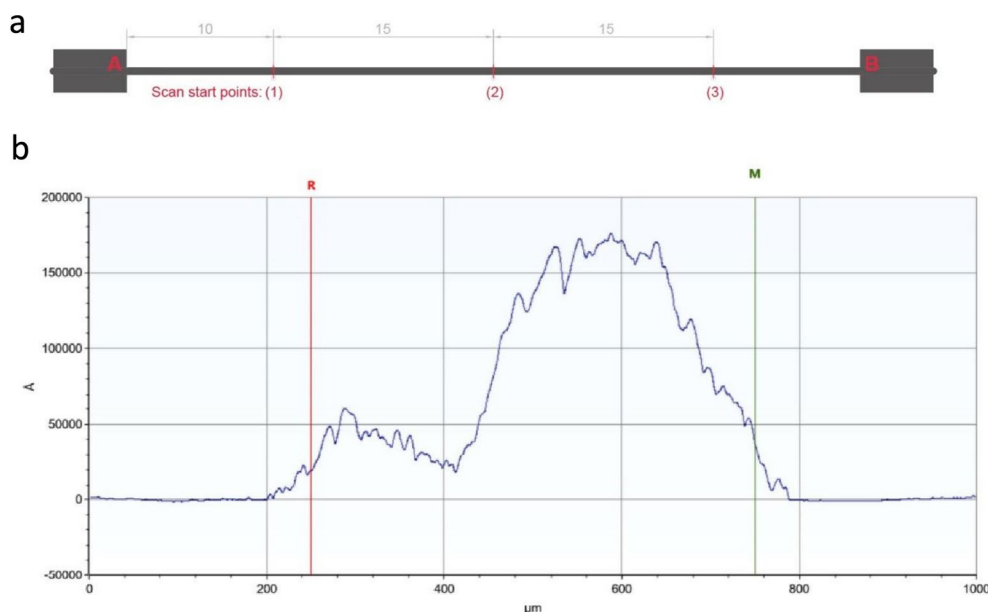


**Figure 7:** Scheme of profilometry measurements: (a) scan layout; (b) representative scan for the print on PET substrate printed with anilox roller 40  $\text{cm}^3/\text{m}^2$ .

substrate were tested. A piece of tesa 4104 tape was applied on a printed surface, pressed to the sample by hand, and then removed from the specimen. The ink adhesion was estimated by the amount of ink removed with adhesive tape. A five-level scale was used for samples rating:

- Level 1: no ink removal.
- Level 2: slight ink removal (< 10%).
- Level 3: moderate ink removal (10–30%).
- Level 4: severe ink removal (30–60%).
- Level 5: almost complete ink removal (> 60%).

### Scratch resistance

Scratch resistance was checked using FINAT method no. 27. Scratch resistance describes the mechanical resistance of a printed surface. Twenty-five samples were tested on each substrate. Testing was performed on an Ink Rub Tester by Testing Machines Inc. The printed sample adhered to the 4 lbs weight. Then label has been scratched against the metallic surface. The used machine setup was 100 moves per minute, 25 cycles for each sample. In the end, the tested sample was observed for ink rub or scratch-off. A five-level scale was used for samples rating:

- Level 1: Slightly scratched surface < 5% damage, no scratch-off, no rub-off, no substrate visible.
- Level 2: Scratched ink film or rubbed off the ink film, < 10% substrate visible.
- Level 3: Scratched ink film or rubbed off the ink film, 10–30% substrate visible.
- Level 4: Scratched ink film or rubbed off the ink film, 30–60% substrate visible.
- Level 5: Scratched ink film or rubbed off the ink film, > 60% substrate visible.

### Bending resistance

Bending tests were performed on Yasa Tension-Free U-shape folding machine. Twenty-five samples were tested on each substrate. The following setup was used: 60 cycles/min, bending radius  $\approx$  20 mm, 600 cycles per sample in total. Electrical conductivity was measured before and after the test. Additionally, the surface of the print was inspected under a microscope. A three-level scale was used for samples rating

- Level 1: no layer damage, resistance remains the same.
- Level 2: slight layer damage, resistance decreasing is noted.
- Level 3: visible cracking of the printed layer, no resistance.

### Electrical testing

The electrical performance of the samples was determined by measuring the sheet resistance, stated conventionally as ohms per square ( $\Omega/\text{sq}$ ). The digital multimeter AXIOMET AX-160IP and two-point measurement method were used. The average value from 25 samples was used for sheet resistance assessment of each tested variation.

### Viscosity tests

The rheology was measured according to the rheometer's specifications, by placing the material sample on the bottom plate with the instrument head in the upper position. After removing excess sample from around the cone, the required temperature was set. The cone was then lowered into position with the gap already set, and the measurement procedure began. The ink shear viscosity was measured with the use of an R/S Plus Rheometer (Brookfield Engineering, Middleboro, MA, USA) equipped with an RCT-50–1 spindle, dedicated to the viscosity ranging between 0006 and 50 900 Pa·s. A shear rate from 0 to 500 1/s for 200 s was used due to the limitation of the viscometer. The constant temperature of  $25 \pm 0.5^\circ\text{C}$  was kept during the measurements. The data were then analyzed using the Rheo 3000 software (Brookfield Engineering, Middleboro, MA, USA). Three replicates were performed for each sample.

### Acknowledgments

This project has received funding from the National Centre for Research and Development, grant number POIR.01.01.01-00-0622/18 and the Institute of Metrology and Biomedical Engineering, Faculty of Mechatronics, Warsaw University of Technology. We would like to acknowledge Mr Kenneth Bell, who checked the manuscript for clarity and accessibility.

### Author contributions

SL-K: conceptualization, methodology, formal analysis, writing—review and editing. TN: investigation, data curation, writing—original draft preparation; KW: investigation, data curation; DJ: investigation, data curation; PW: investigation, data curation; MJ: supervision, funding acquisition.

### Funding

The present paper is financially supported by the National Centre for Research and Development, grant number POIR.01.01.01-00-0622/18 and the Institute of Metrology and Biomedical Engineering, Faculty of Mechatronics, Warsaw University of Technology.

## Data availability

Data available upon request.

## Declarations

**Conflict of interest** On behalf of all authors, the corresponding author states that there is no conflict of interest.

## Open Access

This article is licensed under a Creative Commons Attribution 4.0 International License, which permits use, sharing, adaptation, distribution and reproduction in any medium or format, as long as you give appropriate credit to the original author(s) and the source, provide a link to the Creative Commons licence, and indicate if changes were made. The images or other third party material in this article are included in the article's Creative Commons licence, unless indicated otherwise in a credit line to the material. If material is not included in the article's Creative Commons licence and your intended use is not permitted by statutory regulation or exceeds the permitted use, you will need to obtain permission directly from the copyright holder. To view a copy of this licence, visit <http://creativecommons.org/licenses/by/4.0/>.

## References

1. Printed Electronics Market Size, Share & Industry Trends Report—2026. Dostęp: 25 wrzesień 2022. Dostępne na: <https://www.marketsandmarkets.com/Market-Reports/printed-electronics-market-197.html>
2. J. Park, K. Shin, L. Changwoo, Roll-to-roll coating technology and its applications: a review. *Int. J. Precis. Eng. Manuf.* **17**, 537–550 (2016). <https://doi.org/10.1007/s12541-016-0067-z>
3. K.H. Choi, J.T. Yoo, C.K. Lee, S.Y. Lee, All-inkjet-printed, solid-state flexible supercapacitors on paper. *Energy Environ. Sci.* (2016). <https://doi.org/10.1039/c6ee00966b>
4. O. El Baradai, Microfibrillated cellulose based ink for eco-sustainable screen printed flexible electrodes in lithium ion batteries. *J. Mater. Sci. Technol.* (2016). <https://doi.org/10.1016/j.jmst.2016.02.010>
5. Q. Huang, Y. Zhu, Printing conductive nanomaterials for flexible and stretchable electronics: a review of materials, processes, and applications. *Adv. Mater. Technol.* (2019). <https://doi.org/10.1002/admt.201800546>
6. Z. Jiang, Reverse-offset printed ultrathin Ag mesh for robust conformal transparent electrodes for high-performance organic photovoltaics. *Adv. Mater.* (2018). <https://doi.org/10.1002/adma.201707526>
7. N. Karim, S. Afroj, S. Tan, K.S. Novoselov, S.G. Yeates, All inkjet-printed graphene-silver composite ink on textiles for highly conductive wearable electronics applications. *Sci. Rep.* (2019). <https://doi.org/10.1038/s41598-019-44420-y>
8. J. Liang, K. Tong, Q. Pei, A water-based silver-nanowire screen-print ink for the fabrication of stretchable conductors and wearable thin-film transistors. *Adv. Mater.* (2016). <https://doi.org/10.1002/adma.201600772>
9. J. Machiels, A. Verma, R. Appeltans, M. Buntinx, E. Ferraris, W. Deferme, Printed electronics (PE) as an enabling technology to realize flexible mass customized smart applications. *Procedia CIRP* **96**, 115–120 (2021). <https://doi.org/10.1016/j.procir.2021.01.062>
10. R.G. Scalisi, Inkjet printed flexible electrodes for surface electromyography. *Org. Electron.* **18**, 89–94 (2015). <https://doi.org/10.1016/j.orgel.2014.12.017>
11. J. Wiklund, A Review on printed electronics: fabrication methods, inks, substrates, applications and environmental impacts. *J. Manuf. Mater. Process* (2021). <https://doi.org/10.3390/jmmp5030089>
12. S. Yao, Y. Zhu, Wearable multifunctional sensors using printed stretchable conductors made of silver nanowires. *Nanoscale* (2014). <https://doi.org/10.1039/c3nr05496a>
13. H.P. Kn, C.S. Meghana, N.K. Raju, S.P. Shilpa, M.R. Yashaswini, C. Manjunatha, Current developments in conductive nano-inks for flexible and wearable electronics. *ECS Trans.* **107**(1), 11261 (2022). <https://doi.org/10.1149/10701.11261ecst>
14. C. MCCALL, Improving the Manufacture by Flexographic Printing of RFID Aerials for Intelligent Packaging.
15. E. Frank, Printing ink—Requirements, possibilities, potentials for optimisation, pp. 42–47, 2005.
16. A.N. Gafurov, Registration error analysis and compensation of roll-to-roll screen printing system for flexible electronics. *Flex. Print. Electron.* **6**(2), 024003 (2021). <https://doi.org/10.1088/2058-8585/abf987>
17. P. Gomes, D. Tama, H. Carvalho, A.P. Souto, Resistance variation of conductive ink applied by the screen printing technique on different substrates. *Color. Technol.* **136**(2), 130–136 (2020). <https://doi.org/10.1111/cote.12451>
18. P. He, Screen-printing of a highly conductive graphene ink for flexible printed electronics. *ACS Appl. Mater. Interfaces* **11**(35), 32225–32234 (2019). <https://doi.org/10.1021/acsami.9b04589>
19. N.X. Williams, S. Noyce, J.A. Cardenas, M. Catenacci, B.J. Wiley, A.D. Franklin, Silver nanowire inks for direct-write electronic tattoo applications. *Nanoscale* **11**(30), 14294–14302 (2019). <https://doi.org/10.1039/C9NR03378E>
20. Challenges of printed electronics on flexible substrates. Dostęp: 25 wrzesień 2022. Dostępne na: <https://ieeexplore.ieee.org/abstract/document/6292087/>
21. D.D. Mariappan, S. Kim, A.J. Hart, A precision desktop plate-to-roll apparatus for development of advanced flexographic printing

- processes. *Precis. Eng.* **66**, 392–400 (2020). <https://doi.org/10.1016/j.precisioneng.2020.07.012>
22. M. Morgan, D. Curtis, D. Deganello, Control of morphological and electrical properties of flexographic printed electronics through tailored ink rheology. *Org. Electron.* (2019). <https://doi.org/10.1016/j.orgel.2019.05.027>
  23. Z.W. Zhong, J.H. Ee, S.H. Chen, X.C. Shan, Parametric investigation of flexographic printing processes for R2R printed electronics. *Mater. Manuf. Process.* **35**(5), 564–571 (2020). <https://doi.org/10.1080/10426914.2020.1732411>
  24. M. Gajadhur, M. Regulska, Mechanical and light resistance of flexographic conductive ink films intended for printed electronics. *Dyes Pigments* **178**, 108381 (2020). <https://doi.org/10.1016/j.dyepig.2020.108381>
  25. A.M. Rodes-Carbonell, J. Ferri, E. Garcia-Breijo, I. Montava, E. Bou-Belda, Influence of structure and composition of woven fabrics on the conductivity of flexography printed electronics. *Polymers* (2021). <https://doi.org/10.3390/polym13183165>
  26. S. Thibert, Silver ink experiments for silicon solar cell metallization by flexographic process. zaprezentowano na Conference Record of the IEEE Photovoltaic Specialists Conference, 2012, pp.002266–002270.; <https://doi.org/10.1109/PVSC.2012.6318049>.
  27. Z. Wang, Development of MnO<sub>2</sub> cathode inks for flexographically printed rechargeable zinc-based battery. *J. Power. Sources* **268**, 246–254 (2014). <https://doi.org/10.1016/j.jpowsour.2014.06.032>
  28. T. Mäkelä, S. Jussila, H. Kosonen, T.G. Bäcklund, H.G.O. Sandberg, H. Stubb, Utilizing roll-to-roll techniques for manufacturing source-drain electrodes for all-polymer transistors. *Synth. Met.* **153**(1–3), 285–288 (2005). <https://doi.org/10.1016/j.synthmet.2005.07.140>
  29. S. Lepak-Kuc, K. Wasilewska, D. Janczak, T. Nowicka, M. Jakubowska, Conductive layers on a shrinkable PET Film by flexographic printing. *Materials* (2022). <https://doi.org/10.3390/ma15103649>
  30. N. Ibrahim, J.O. Akindoyo, M. Mariatti, Recent development in silver-based ink for flexible electronics. *J. Sci. Adv. Mater. Devices* (2022). <https://doi.org/10.1016/j.jsamd.2021.09.002>
  31. K. Thiyagarajan, S. G. Rahul, G. K. Rajini, D. Maji, A. Chandrasekhar, Conductive Nanomaterials for Printed and Flexible Electronics Application. *Nanotechnology in Electronics*, (Wiley, 2023) <https://doi.org/10.1002/9783527824229.ch7>.
  32. N. Macadam, 100 m min<sup>-1</sup> industrial-scale flexographic printing of graphene-incorporated conductive ink. *Adv. Eng. Mater.* (2022). <https://doi.org/10.1002/adem.202101217>
  33. R.R. Tafoya, Morphology and electrical properties of high-speed flexography-printed graphene. *Microchim. Acta* (2022). <https://doi.org/10.1007/s00604-022-05232-6>
  34. N. Anzar, Electrochemical sensor for bilirubin detection using paper-based screen-printed electrodes functionalized with silver nanoparticles. *Micromachines* (2022). <https://doi.org/10.3390/mi13111845>
  35. K. Rajan, I. Roppolo, A. Chiappone, S. Bocchini, D. Perrone, A. Chiolerio, Silver nanoparticle ink technology: state of the art. *Nanotechnol. Sci. Appl.* (2016). <https://doi.org/10.2147/NSA.S68080>
  36. J. Zhang, Silver nanoparticles for conductive inks: from synthesis and ink formulation to their use in printing technologies. *Metals* (2022). <https://doi.org/10.3390/met12020234>
  37. I.J. Fernandes, Silver nanoparticle conductive inks: synthesis, characterization, and fabrication of inkjet-printed flexible electrodes. *Sci. Rep.* (2020). <https://doi.org/10.1038/s41598-020-65698-3>
  38. K. Wu, Screen printing of silver nanoparticles on the source/drain electrodes of organic thin-film transistors. *Org. Electron.* **106**, 106524 (2022). <https://doi.org/10.1016/j.orgel.2022.106524>
  39. S. Lepak-Kuc, Ł. Nowicki, D. Janczak, M. Jakubowska, The Influence of the matrix selection and the unification process on the key parameters of the conductive graphene layers on a flexible substrate. *Materials* (2023). <https://doi.org/10.3390/ma16031238>
  40. Q. Muchao, F. Nilsson, Y. Qin, G. Yang, Y. Pan, X. Liu et al., Electrical conductivity and mechanical properties of melt-spun ternary composites comprising PMMA, carbon fibers and carbon black. *Compos. Sci. Technol.* **150**, 24–31 (2017). <https://doi.org/10.1016/j.compscitech.2017.07.004>
  41. D. Murawski, H. Behrens, Effect of particle size and pretreatment on the conductivity of glass powder during compaction. *Z. Für Phys. Chem.* **231**(7–8), 1323–1343 (2017). <https://doi.org/10.1515/zpch-2016-0926>
  42. E. Yuliza, R. Murniati, A. Rajak, K. Khairurrijal, M. Abdullah, Effect of Particle Size on the Electrical Conductivity of Metallic Particles. (2014). <https://doi.org/10.2991/icaet-14.2014.37>.
  43. Influence of particle size and shape on electrical and mechanical properties of graphite reinforced conductive polymer composites for the bipolar plate of PEM fuel cells. Dostęp: 29 grudzień 2022. Dostępne na: <https://www-1.tandfonline-1.com/10000bdge3f0f.eczyt.bg.pw.edu.pl/doi/epdf/https://doi.org/10.1163/156855106776829356?needAccess=true&role=button>
  44. H. Kipphan, in *Handbook of Print Media*, ed. H. Kipphan (Springer, Berlin, 2001) <https://doi.org/10.1007/978-3-540-29900-4>.
  45. S. Kirkpatrick, Percolation and conduction. *Rev. Mod. Phys.* **45**(4), 574–588 (1973). <https://doi.org/10.1103/RevModPhys.45.574>
  46. D.A. Roberson, R.B. Wicker, L.E. Murr, K. Church, E. MacDonald, Microstructural and process characterization of conductive traces printed from Ag particulate inks. *Materials* (2011). <https://doi.org/10.3390/ma4060963>
  47. M. Sangermano, A. Chiolerio, G. Marti, P. Martino, UV-cured acrylic conductive inks for microelectronic devices. *Macromol.*

- Mater. Eng. **298**(6), 607–611 (2013). <https://doi.org/10.1002/mame.201200072>
48. W. Yang, E.J.W. List-Kratochvil, C. Wang, Metal particle-free inks for printed flexible electronics. *J. Mater. Chem. C* **7**(48), 15098–15117 (2019). <https://doi.org/10.1039/C9TC05463D>
49. A. Schwab, R. Levato, M. D'Este, S. Piluso, D. Eglin, J. Malda, Printability and shape fidelity of bioinks in 3D bioprinting. *Chem. Rev.* **120**(19), 10850–10877 (2020). <https://doi.org/10.1021/acs.chemrev.0c00084>
- Publisher's Note** Springer Nature remains neutral with regard to jurisdictional claims in published maps and institutional affiliations.